Swelling of Poly(methyl Methacrylate) Thin Films in Low Molecular Weight Alcohols

J. S. PAPANU,* D. W. HESS, D. S. SOANE (SOONG), and A. T. BELL, *Department of Chemical Engineering, University of California, Berkeley, California 94720*

Synopsis

The effects of solvent size, temperature, and polymer molecular weight on the swelling of poly(methyl methacrylate) (PMMA) thin films in low molecular weight alcohols were investigated using an *in situ* ellipsometer. Apparent activation energies were indicative of non-Fickian diffusion, although optical data showed substantial Fickian character for swelling in methanol and moderate Fickian character in ethanol. Penetration rates were strongly dependent on the solvent molar volume for methanol, ethanol, and isopropanol, but 1-butanol and 2-pentanol had rates similar to isopropanol. The effective cross sections of these longer molecules are similar to isopropanol, and this apparently explains the similar penetration rates. The effect of polymer molecular weight (MW) on methanol penetration rates (21–27°C) was investigated with monodisperse PMMA (M_n = 6.4–40.0 × 10^4 g/mol). A minimum at intermediate MW was observed. Isopropanol swelling rates (45–52°C) were insensitive to MW. The swelling data were also used to determine parameters for transport models that describe the swelling of thin polymer films.

INTRODUCTION

Thin polymer films (~ 1000 nm) are used as resists for lithographic image transfer in the fabrication of microelectronic devices. The resolution and sensitivity of a resist/developer–solvent system are strongly influenced by solvent transport in the polymer. A parametric study of resist swelling can provide a better understanding of solvent transport processes. By using solvents which swell but do not dissolve the films, solvent transport can be isolated from polymer dissolution effects. The insight gained from swelling studies could be useful for improving resolution.

Swelling results from the penetration of solvent into the polymer. Solvent penetration consists of two processes—diffusion of solvent molecules into the polymer matrix and local relaxation of polymer segments. The characteristic times for diffusion and relaxation (and the changes in these characteristic times as the film swells) determine whether normal Fickian transport is observed.[1] Often with glassy polymers, a sharp front between unpenetrated and swollen polymer propagates into the film at a constant rate. This type of non-Fickian transport is referred to as Case II diffusion.[2]

With Case II transport, solvent transport in the swollen region still proceeds by Fickian diffusion.[3-5] In thinner films, the diffusional resistance of the swollen polymer (gel) is negligible, and swelling is always limited by solvent

*Current address is Philips Research Laboratories, Sunnyvale, Signetics Corporation, Sunnyvale, CA 94088.

Journal of Applied Polymer Science, Vol. 39, 803–823 (1990)
 CCC 0021-8995/90/040803-21$04.00

penetration at the front. In thicker films, the diffusional resistance of the swollen region increases as the film swells, and Fickian diffusion of solvent between the polymer–solvent interface and the penetrating front may eventually control the swelling kinetics. Consequently, an apparent shift to Fickian transport can occur with thicker films.[3]

A similar shift in the apparent transport mechanism can result from an increase in temperature (for sufficiently thick films).[3] If the temperature is raised, both the penetration rate of the front and the diffusivity of solvent in the swollen region increase. However, the increase in the front penetration rate is more significant than the increase in solvent diffusivity because the apparent activation energy for front penetration is higher than that for solvent diffusion.[4] Thus, the effective diffusional resistance of the swollen region is increased.

Poly(methyl methacrylate) (PMMA) is used as a positive-tone electron-beam resist and is typically developed in a ketone/alcohol solvent mixture. In the absence of ketones, alcohols slowly swell the polymer, but, in ketone/alcohol mixtures, alcohols act as nonsolvents and moderate the dissolution rate of unexposed regions. This moderation improves process control and enhances contrast between the exposed and unexposed regions. Several studies of PMMA thin films dissolving in ketones[6–9] and ketone/alcohol mixtures[7,10] have been reported, but few[10] results have been published for swelling in pure alcohols.

Swelling of sheet PMMA in lower molecular weight (MW) alcohols has been reported, however. The transport of methanol (MeOH) in 1 and 3 mm thick PMMA at 23–63°C showed Case II behavior for thinner samples and lower temperatures.[3] Fickian behavior was observed at elevated temperatures and also at long times for thicker samples. These observations can be explained in terms of activation energies and diffusional resistances as discussed above. Swelling data[11] for sheet PMMA in MeOH, ethanol (EtOH), isopropanol (IpOH), and *n*-propanol (POH) at 20 and 45°C have been analyzed[12] and found to correspond to Case II uptake. Similarly, 2 mm thick PMMA sheets swelling in EtOH, POH, and 1-butanol between 50 and 95°C showed Case II diffusion near 50°C, but at higher temperatures the penetration had Fickian character.[4]

No studies have been reported on the effect of polymer MW on PMMA swelling rates. It would be useful to understand how MW affects penetration rate since it has been found that the dissolution rate of PMMA films in methyl isobutyl ketone decreases with increasing polymer MW and that the dissolution rate is controlled by solvent penetration.[6] One problem with studying the effect of MW is the difficulty in isolating any inherent dependence of penetration rate on polymer MW from sample preparation effects. For example, if films are annealed during preparation, the response time during subsequent quenching will depend on polymer MW. Differences in free volume and consequently the penetration rate could result. Such problems have led to contradictory results for studies with polystyrene.[13,14]

The primary objectives of this paper were to identify the mechanisms and quantify the penetration kinetics of low MW alcohols in thin PMMA films. *In situ* ellipsometry was used to monitor swelling. The effects of solvent size, temperature, and polymer MW on swelling were investigated. Also, parame-

ters for Fickian and Case II transport models were determined from the ellipsometry data. These models describe the swelling of thin polymer films and are reported elsewhere.[15]

EXPERIMENTAL

Materials and Sample Preparation

Both monodisperse and polydisperse PMMA were used in our studies. The polydisperse material was KTI Chemicals 950K e-beam resist, a 6 wt % solution of PMMA in chlorobenzene (M_n = 180,000 g/mol and M_w/M_n = 2.8 from GPC analysis). Monodisperse PMMA solutions were prepared by dissolving MW standards (Polysciences, Scientific Polymer Products, Pressure Chemical, and Polymer Laboratories) in chlorobenzene to yield solutions of 5–15 wt to vol % polymer. The polymer solutions were spin-coated at 500–2000 rpm onto Si wafers (cleaned in 5 : 1 by volume $H_2SO_4 : H_2O_2$ and dipped in 10 : 1 H_2O : 49% HF). After spinning, the samples were baked at 160°C for 1 h in a convection oven and then ambient quenched at 19–22°C. Film thickness ranged from 300 to 2000 nm, although most films were approximately 1000 nm thick. Reagent grade MeOH, EtOH, IpOH, 1-butanol, and 2-propanol were used for the swelling studies.

Ellipsometer

Ellipsometry measures the relative change in polarization state of a light beam as it reflects from a bare or film-covered substrate. The electric fields of the incident and reflected beams are described, respectively, by the complex amplitudes E_i and E_r.[16] Each complex amplitude can be resolved into components parallel (p) and perpendicular (s) to the plane of incidence, the reference plane defined by the incident and reflected beams. The fundamental equation of ellipsometry is[16]

$$\rho = \frac{E_{r,p}/E_{i,p}}{E_{r,s}/E_{i,s}} = \tan(\psi)\exp(i\Delta) \tag{1}$$

where ρ is the overall reflection coefficient and the parameters Δ ($-180° \leq \Delta \leq 180°$) and ψ ($0° \leq \psi \leq 90°$) relate, respectively, to the relative phase and amplitude changes upon reflection. For a thin polymer film cast on a substrate and immersed in a solvent, Δ and ψ will be functions of the refractive indices of the polymer, solvent, and substrate, the thickness of the film, the solvent concentration profile within the film, the wavelength of the light source, and the angle of incidence (measured with respect to a perpendicular to the plane of the film).

For the studies reported here, a rotating-analyzer ellipsometer[17] was used to measure values of Δ and ψ (typically at intervals of 5–60 s). This instrument is described in detail elsewhere.[18] Briefly, the sample is placed in a thermally regulated (± 0.2°C) optical cell which permits immersion in solvent and passage of the incident and reflected light beams via quartz windows. The aluminum cell is wrapped with heating tape and insulated. A heating element

cannot be used directly in the cell since the resulting convective currents cause intolerable signal fluctuations. The solvent is either stagnant or circulated at up to 30 mL/min with a magnetic pump. Studies above room temperature were typically performed with stagnant solvent to allow for more rapid temperature equilibration. For runs near or below room temperature, the solvent was pumped from a reservoir through heat exchange baths and into the bottom of the cell.

DATA ANALYSIS

Data Interpretation

The average penetration rate was calculated by dividing the initial film thickness by the time required for the film to swell completely (reach equilibrium). Complete swelling was marked by values of Δ and ψ that were time-invariant. Some second-order swelling was often evident, as indicated by slight changes in Δ and ψ after equilibrium (primary) had been reached. This solvent uptake was insignificant, however, relative to the overall mass uptake, and was most likely due to secondary relaxations of polymer segments. In most cases, only the average penetration rate was desired. For more detailed analysis, swelling data were interpreted by the use of transport[15] and optical[19,20] models which generate predicted values of Δ and ψ vs. time.

The transport models describe the swelling of thin polymer films by providing concentration profiles and boundary locations as functions of time. Two separate transport models were developed,[15] one for Fickian diffusion and one for Case II penetration. The Fickian model has a continuous concentration (solvent volume fraction ϕ_1) profile and one moving boundary, the polymer–solvent interface, which moves outward as the solvent penetrates [Fig. 1(a)]. The Case II model has two moving interfaces, the front between unpenetrated polymer and the swollen gel layer, and the polymer–solvent interface [Fig. 1(b)]. The front moves inward and the polymer–solvent interface moves outward as the polymer swells. Between the front and the polymer–solvent interface, the time and position dependence of ϕ_1 are described by Fickian diffusion. The ellipsometric parameters Δ and ψ are calculated from the concentration profiles and boundary locations by approximating the film as a stack of thin, discrete layers. The refractive index of each layer is determined from the local solvent concentration and mixing rules.[21] The overall reflection coefficient [eq. (1)] is determined by summing the contribution of each interface, starting at the polymer-substrate interface.[20]

In the optical models, swelling is simulated by varying in a prescribed manner the thickness of layers which are stacked on a substrate. For example, Case II transport can be approximated with a two-layer optical model. The underlying layer has the refractive index of the glassy polymer, and the thickness of this layer decreases with time from the initial film thickness to zero. The upper layer has the refractive index of the swollen layer and increases in thickness from zero to the equilibrium swollen thickness. (This two-layer model assumes that the solvent concentration profile in the swollen region is flat, i.e., the diffusional resistance is negligible.) As with the transport models, Δ and ψ are calculated by summing the contribution of each interface

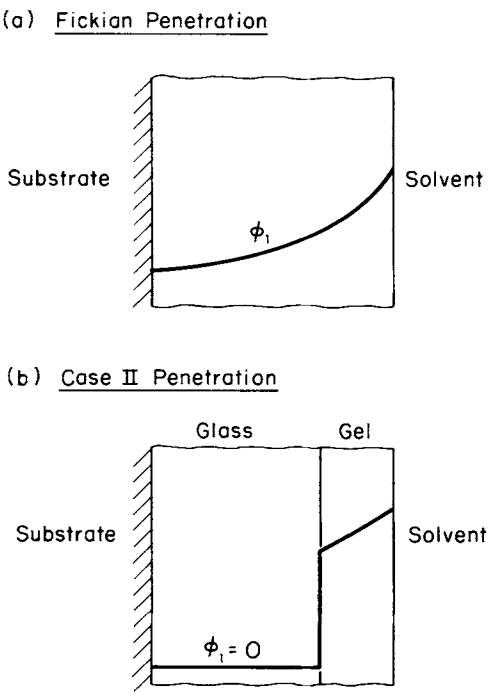

Fig. 1. Interface positions and concentration profiles for (a) Fickian and (b) Case II transport models.

to the overall reflection coefficient. The optical models are less computationally intensive since partial differential equations are not solved and since typically far fewer layers are used to approximate the film. However, the optical models are not very useful for estimating Fickian penetration since the concentration profiles must first be obtained from solution of a nonlinear diffusion equation.[15]

The experimental data were fit either by manual iteration or by search routines with the set of model (transport or optical) parameters that minimize the objective function S,

$$S = \left\{ \frac{1}{N-1} \sum_{i=1}^{N} \left[(\Delta_c - \Delta_e)_i^2 + (\psi_c - \psi_e)_i^2 \right] \right\}^{1/2} \tag{2}$$

where the subscripts c and e refer to "calculated" and "experimental," respectively, and N is the number of data points. For the results presented in this paper, eq. (2) was applied in the determination of solvent diffusivities and equilibrium solvent concentrations.

Case II Model Parameters

The Case II model parameters are particular to the model[5,15] used to describe this phenomenon. Consequently, a brief description of this model follows. The velocity of the penetrating front, v, is assumed to be stress

driven, and is given by[5]

$$v = -K(a\pi - \sigma_c) \tag{3}$$

where K is a front factor, a is an amplification factor (usually $\pi < \sigma_c$), π is the osmotic pressure due to the presence of the imbibed solvent, σ_c is the critical stress level needed to initiate front movement, and the positive direction is away from the substrate toward the solvent. Equation (3) is based on an analogy to crazing (formation of microcracks) driven by mechanical stress,[5] and the parameter σ_c can be thought of as the stress level needed for crazing to occur. Thus, σ_c can be estimated from mechanical crazing data, and is assumed to be a linear function of temperature,[5]

$$\sigma_c = \gamma(T_g - T) \tag{4}$$

where γ is a constant and T_g is the glass transition temperature. The parameter K is assumed to depend only on the properties of the pure polymer and temperature [$K \sim \exp(-E_a/RT)$, where E_a is the apparent activation energy and R is the gas constant], and can be determined from either mechanical crazing or swelling data. The osmotic pressure is given by Flory–Huggins theory,[22]

$$\pi = \frac{RT}{V_1}\left[\phi_1 - \chi\phi_1^2 - \frac{1}{X}\ln(1 - \phi_1)\right] \tag{5}$$

where V_1 is the molar volume of the solvent, χ is the Flory–Huggins interaction parameter, and X is the ratio of the molar volume of the polymer to that of the solvent. It follows from eqs. (3) and (5) that the front velocity increases with solvent concentration. After values of K, π, and σ are estimated, the amplification factor a is calculated from the solvent penetration rate and eq. (3). To a first approximation, a is assumed to be a function of temperature only.[5] However, any dependence of penetration rate on solvent that is not accounted for in π will be included in a.

Optical Constants

Data interpretation requires accurate values of the refractive index for the substrate, film, and solvent. The optical constants of Si have been tabulated[23,24] for various wavelengths. A value of $N = 3.85 - i0.02$ at 633 nm was used in this study, since this value is more appropriate when a native oxide is present on the surface of the Si wafers.

Refractive index measurements of 1000 nm PMMA films on Si substrates (in air) with our ellipsometer yielded indices of 1.48–1.50. A value of 1.489 at 20°C and 633 nm was used in the calculations. This agrees favorably with other published data for bulk PMMA[25,26] ($n = 1.489$), integrated optical measurements of PMMA thin films[27] ($n = 1.4856$), and ellipsometric measurements of 300–2000 nm films spun onto GaAs[28] and InP[29] substrates ($n =$ 1.45–1.55). The refractive index was corrected for temperature using a value of $-1.3 \times 10^{-4}/°C$[26] for the temperature coefficient, dn/dT. This value of

dn/dT corresponds to unconstrained polymer, and the magnitude may be somewhat lower for spun-on films which are constrained at the polymer–substrate interface.

For the solvents of interest, refractive indices were obtained from the literature,[30,31] manufacturers' data, and measurements. Refractive index data near 20°C for several wavelengths[30] were used to estimate dispersion effects for each solvent so that refractive index values could be corrected to 633 nm. Also, the refractive index as a function of temperature was measured between 19 and 55°C using a temperature-controlled Abbé refractometer (589 nm). The refractive index decreased linearly with temperature over this temperature range, and dn/dT values agreed favorably with literature values.[30,32] The temperature corrections at 589 nm were assumed to be applicable at 633 nm, and the dispersion correction near 20°C were assumed to be applicable over the entire temperature range investigated.

Refractive indices of polymer–solvent mixtures were needed to determine the composition of swollen films. Direct calibration measurements with mixtures were not performed, however, due to the large number of solvent, composition, and temperature combinations needed for all systems studied. Instead, refractive indices were approximated by using the optical constants of the pure solvent and polymer, and applying the Maxwell–Garnett mixing rule.[21] This mixing rule is based on a Lorentz-Lorenz type equation for dielectric properties,[21]

$$\frac{\epsilon_f - \epsilon_h}{\epsilon_f + 2\epsilon_h} = \sum_{i=1}^{n} \phi_i \frac{\epsilon_i - \epsilon_h}{\epsilon_i + 2\epsilon_h} \tag{6}$$

where ϵ_f is the effective dielectric function (complex) of the film, ϵ_h is the dielectric function of the host, ϵ_i is the dielectric function of component i ($\epsilon_i = N_i^2$, where N_i is the complex refractive index of component i), and n is the number of components. The Maxwell–Garnett mixing rule assumes that the host is the most abundant pure component. Both the polymer and solvent were assumed to be nonabsorbing, so that their refractive indices simplified to real values.

RESULTS AND DISCUSSION

Penetration Mechanism

Traces of ψ and Δ vs. time for polydisperse PMMA (1340 nm) swelling in MeOH at 19.0°C are shown in Figures 2a and 2b. Theoretical curves generated from the Fickian and Case II transport models are presented in Figures 2(c), (d) and 2(e), (f), respectively. The distinct differences in Δ and ψ between the two models are due to the presence of the second sharp interface with the Case II model. Clearly, the experimental data follow the Fickian model more closely.

Based on previous experimental studies[3] with sheet PMMA, Case II behavior is expected for the temperatures considered in our study. The Fickian behavior observed here suggests a thin-film effect. One possible explanation for the Fickian behavior is that the initial uptake of MeOH is Fickian. With

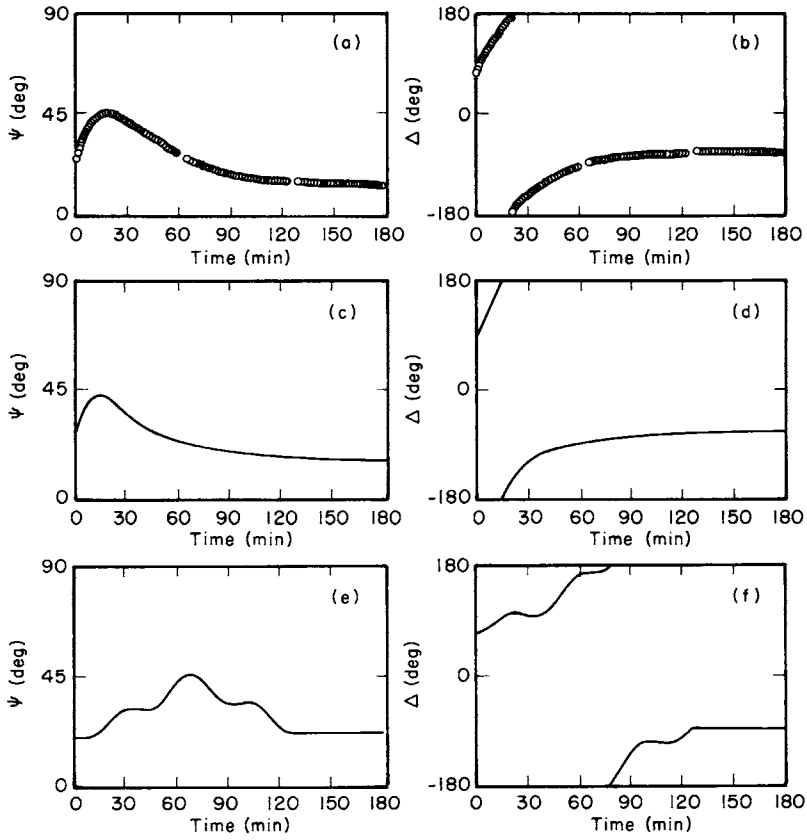

Fig. 2. (a, b) Experimental ψ and Δ for methanol penetration at 19.0°C. Initial thickness = 1350 nm. (c, d) Values of ψ and Δ for MeOH penetration predicted by the Fickian model. (e, f) Values of ψ and Δ for MeOH penetration predicted by the Case II model.

sheet samples, observations are made well after the solvent has penetrated the first 1000 nm of the film, so that only a sharp front is seen. With thin films, this initial Fickian uptake could be a major fraction of the overall swelling. Similar effects of film thickness on the mechanism of solvent penetration have been observed with *n*-alkane swelling of polystyrene.[33] For conditions at which Case II sorption was observed in 7.5×10^4 nm films and 1.84×10^5 nm spheres, absorption in 534 nm microspheres was Fickian. The author suggests that for very thin samples a sharp front never has a chance to be established.

Another possible explanation for the apparent Fickian behavior is infiltration of the relatively small MeOH molecules ahead of the Case II front. It is known that with Case II diffusion, a Fickian precursor[34] precedes the penetrating front, and this precursor could be significant for MeOH. Furthermore, for thin films, the precursor could constitute a major portion of the overall thickness. Infiltration ahead of the front would result in a diffuse interface, but penetration would still be controlled by a Case II mechanism. Although it is difficult to differentiate between an initial Fickian uptake and substantial infiltration of the solvent ahead of a Case II front, either process would explain the thin film effects seen with MeOH penetration.

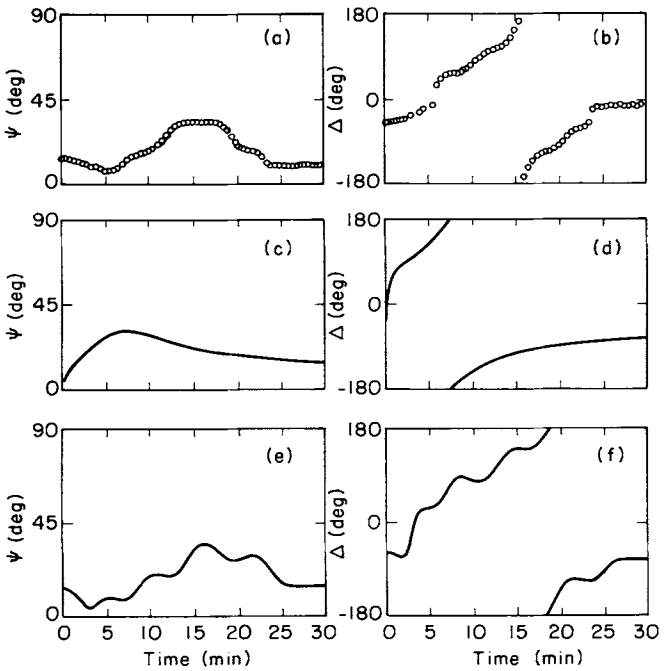

Fig. 3. (a, b) Experimental ψ and Δ for ethanol penetration at 40.8°C. Initial thickness = 1740 nm. (c, d) Values of ψ and Δ for EtOH penetration predicted by the Fickian model. (e, f) Values of ψ and Δ for EtOH penetration predicted by the Case II model.

Representative plots of Δ and ψ for swelling in EtOH (40.8°C) and IpOH (50.1°C) along with predicted plots from the Fickian and Case II models are presented in Figures 3(a)–(f) and 4(a)–(f). The traces for EtOH shown in Figure 3 suggest that the penetration is Case II. However, some Fickian character (diffuse interface) is evident by the smoothing of the sharp wiggles predicted by the Case II model. Figure 4 shows that IpOH penetration is strongly Case II. The progression from Fickian to Case II swelling can be ascribed to the increasing molecular size of the penetrant. With the larger molecules, appreciable infiltration of the solvent ahead of the front will be difficult, and a sharp front can be maintained. It should be noted that, although higher temperatures were used for the higher MW solvents in Figures 2–4 (to give reasonable penetration rates), mechanistic differences between the solvents were still seen at a fixed temperature. Thus, the transition in diffusion mechanism seen in Figures 2–4 is a consequence of the progressively larger size of the solvent molecules, not higher temperatures.

For the most part, the penetration mechanism for each solvent remained unchanged over the thickness, temperature, and molecular weight ranges investigated. It should be emphasized, however, that some superposition of the less dominant mechanism was always present. A duality in the diffusion mechanism can be seen to a small extent with IpOH swelling. Close examination of Figure 4 reveals that the experimental curves are smoothed out relative to the undulations predicted, assuming a perfectly sharp interface between the unpenetrated glass and the swollen region [compare Figs 4(a) and

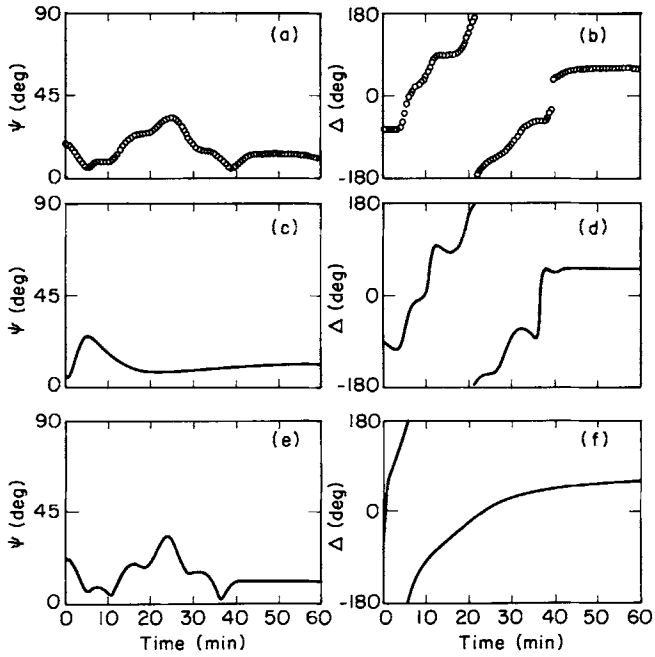

Fig. 4. (a, b) Experimental ψ and Δ for isopropanol penetration at 50.1°C. (c, d) Values of ψ and Δ for IpOH penetration predicted by the Fickian model. (e, f) Values of ψ and Δ for IpOH penetration predicted by the Case II model.

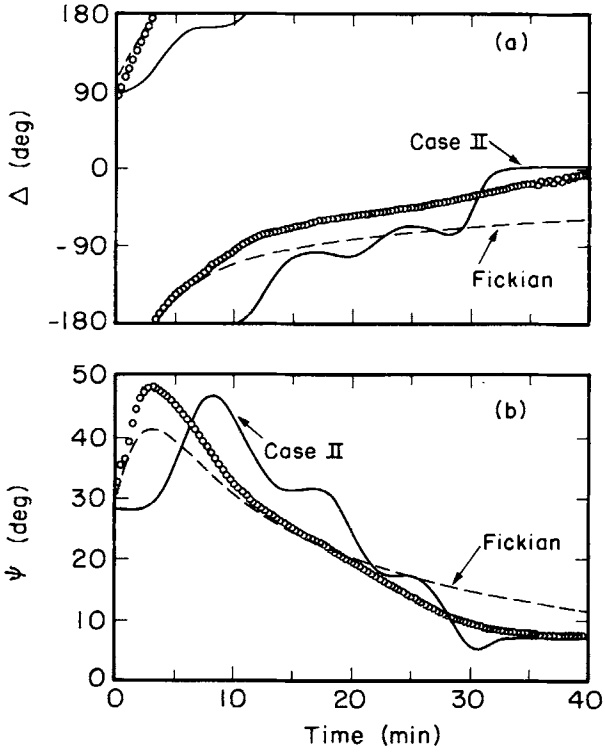

Fig. 5. Experimental and predicted (a) ψ and (b) Δ for methanol penetration at 25.8°C. A Fickian prediction for a concentration independent diffusivity of 1.0×10^{-11} cm^2/s and a pseudo Case II (optical model) prediction are shown. The equilibrium solvent volume fraction is 0.27.

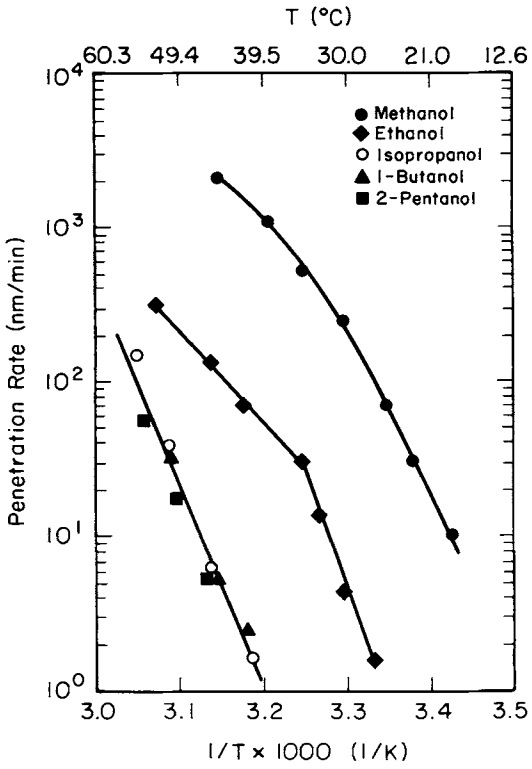

Fig. 6. Average penetration rate vs. $1/T$ for polydisperse PMMA in various alcohols.

4(e) at 20 min]. In addition, some variation in the degree to which one mechanism dominated was observed from sample to sample. For example, the distinct Fickian behavior depicted in Figure 2 was not observed in all MeOH experiments. Figure 5 shows data for MeOH uptake at 25.8°C. Also shown are predicted data from Fickian transport and Case II optical models. Note that the Fickian model predicts an amplitude for ψ which is too low and also predicts an approach to equilibrium which is much less abrupt than the data. While penetration is initially Fickian, some Case II character is evident in later stages of the experiment. (At first, the Case II curves lag behind the experimental curves because the predicted curves correspond to solvent uptake which is linear in time and accompanied by a sharp interface.) The higher degree of Case II character seen in Figure 5 relative to Figure 2 could be attributable to the temperature increase from 19.0 to 25.8°C. However, variations in the degree to which the primary mechanism dominated were seen from sample to sample (perhaps due to residual stresses), and thus it cannot be concluded that the decrease in Fickian character correlates with an increase in temperature.

Temperature

The average penetration rate for each alcohol in polydisperse PMMA is plotted vs. $1/T$ in Figure 6. The apparent activation energies clearly decrease with increasing temperature. Table I summarizes approximate activation

TABLE I
Apparent Activation Energies for Polydisperse PMMA Swelling in Various Alcohols

Alcohol	Temperature range (°C)	Activation energy (kcal/mol)
Methanol	19.0–30.2	48
Methanol	30.2–38.5	33
Ethanol	26.2–35.0	60
Ethanol	35.0–45.0	26
2-Propanol	40.1–50.1	59
1-Butanol	40.8–50.0	59
2-Pentanol	45.5–53.3	59

energies over several temperature ranges. (These activation energies cannot be ascribed solely to the dynamics of penetration since the equilibrium solvent concentration and consequently the osmotic pressure in the Case II model increases with temperature.) There does not appear to be a correlation between molecular size and activation energy. While the optical data (Fig. 2) indicate a high degree of Fickian behavior for MeOH penetration, the activation energies are consistent with Case II behavior.[3,4] This suggests that a front which is diffuse due to initial Fickian swelling and/or solvent infiltration propagates into the film.

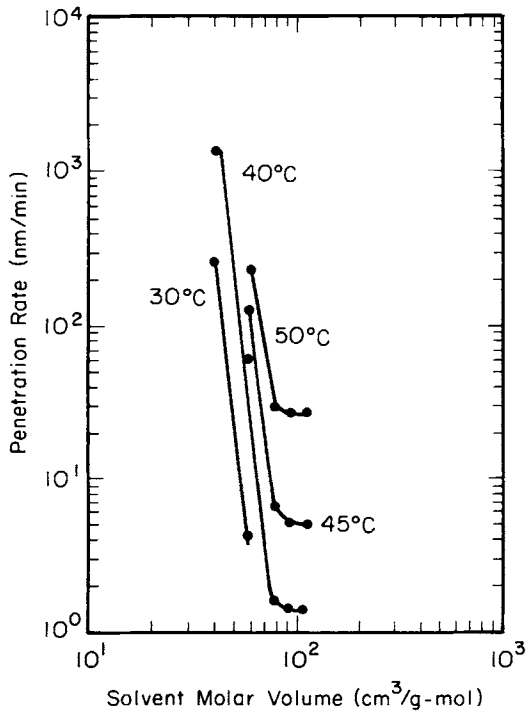

Fig. 7. Average penetration rate vs. solvent molar volume at several temperatures.

Solvent Size

As seen in Figure 6, the smaller molecules are kinetically more favorable, and penetrate at significantly higher rates, as expected. An approximate measure of molecular size is molar volume, and plots of log penetration rate (interpolated) vs. log molar volume at several temperatures are shown in Figure 7. The curves show a sharp drop in rate as molar volume increases, and then level off for 1-butanol and 2-pentanol. Apparently, the effective cross section of a molecule is more significant in determining penetration rate than its molar volume. This is reasonable since longer molecules of comparable cross section can align themselves such that their longer backbone does not hinder diffusion.

Polymer Molecular Weight

Figure 8 shows the log of average penetration rate vs. $1/T$ for monodisperse and polydisperse samples swelling in MeOH. The data suggest a dependence on MW and polydispersity. Consider the monodisperse samples first. For polymer molecular weights of 1.42×10^5 and 2.65×10^5 g/mol, the data lie along the same line, indicating comparable rates for these two MWs, but the

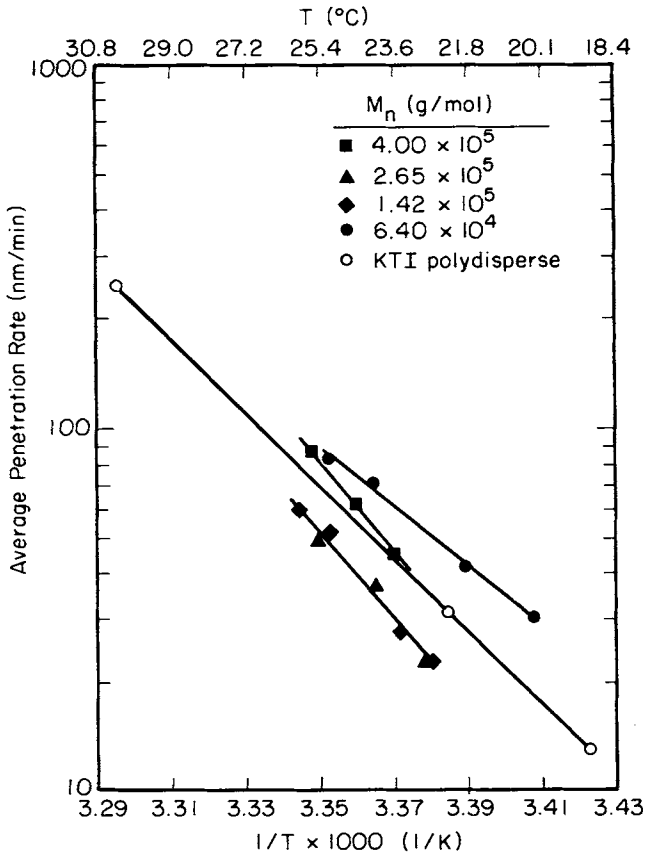

Fig. 8. Average penetration rate vs. $1/T$ for monodisperse and polydisperse PMMA in MeOH.

6.4×10^4 g/mol data show higher penetration rates. If the rate differences were due to free volume effects resulting from the ambient quench,[6] the lower MW material would have a lower free volume and consequently a lower penetration rate. Thus, it appears that there is an intrinsic dependence on MW at lower MW which levels off somewhere above 1×10^5 g/mol. As the molecular weight is increased to 4.0×10^5 g/mol, however, the rate increases. We believe that the higher rate is a free volume effect which is due to the ambient quench, and which becomes noticeable at higher MW. Finally, penetration rates in polydisperse ($M_n = 1.8 \times 10^5$ g/mol) resist are between those for the 6.4×10^4 and the 1.42×10^5 g/mol (and 2.65×10^5 g/mol) films. Thus, for a particular M_n, polydispersity favors higher penetration rates, which is consistent with the effect of polydispersity seen for PMMA dissolving in methyl isobutyl ketone.[6] Apparently, the low MW tail plays a dominant role in facilitating solvent penetration.

The dependence of penetration rate on polymer molecular weight (at lower MW) further indicates that MeOH penetration has non-Fickian character. If the diffusion mechanism were purely Fickian, no molecular weight-dependence would be expected.[35] In Fickian diffusion, solvent molecules jump along the segments of the polymer chain, and this process is independent of chain length.

The intrinsic dependence of the MeOH penetration rate on polymer MW can be analyzed in terms of the osmotic stress caused by the presence of solvent. It is conceivable that at low MW the polymer film has difficulty supporting the solvent-induced (osmotic) stress, and the stress stretches open the polymer matrix, leading to a higher penetration rate. As the MW increases, the film becomes more capable of supporting the solvent-induced stress, and the solvent penetration rate decreases. At sufficiently high MW (10^5 g/mol), the film can readily support the stress, and the intrinsic penetration rate is independent of polymer MW. These effects can be incorporated into the Case II model by making σ_c dependent on polymer MW.[15] (The Case II penetration rate also depends on molecular weight indirectly through the molar volume ratio X, which influences both ϕ_1^* and π. For MWs applicable to our studies, however, these contributions are negligible.) It has been found[36] that, for mechanical crazing, σ_c is relatively independent of MW over the range $1.2–22.0 \times 10^5$ g/mol. The penetration rate for MeOH levels off at approximately the lower end of this range, and it is conceivable that σ_c decreases with MW below 1.0×10^5 g/mol. A σ_c which increases with MW and then levels off is consistent with the surface fracture energy for PMMA[37] (crazing is a precursor to fracture).

The molecular weight effect was also investigated for PMMA swelling in IpOH at 25–50°C (Fig. 9). With IpOH, no molecular weight effect was observed. Relative to MeOH experiments, the solvent size was larger and temperatures were higher in the IpOH runs. The absence of a MW effect with IpOH is not attributable solely to its larger size because the penetration of methyl isobutyl ketone (an even larger molecule) in PMMA at 24.8°C is dependent on polymer MW.[6] It is likely that the higher temperature was the more significant factor. At higher temperatures, the polymer chain segments can relax more rapidly, which would permit the film to more readily accommodate solvent-induced stress. It should be emphasized that while MW effects

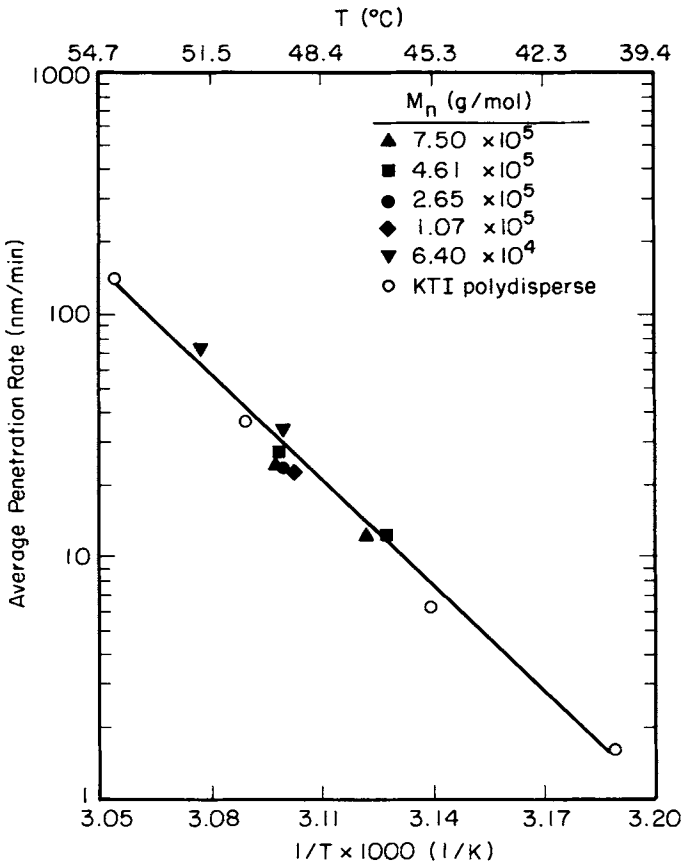

Fig. 9. Average penetration rate vs. $1/T$ for monodisperse and polydisperse PMMA in IpOH.

would not be observed for purely Fickian diffusion, a penetration rate that is independent of polymer MW does not necessarily imply Fickian behavior.

Cracking

Film cracking was observed with 2.7×10^4, 7.2×10^4, and 1.07×10^5 g/mol monodisperse samples swelling in MeOH. Initially, the swelling proceeded at typical rates, and then the film abruptly ruptured. Upon cracking, the reflected laser beam became very diffuse. When the films were removed from the solvent, they had a distinctly different appearance than the uncracked samples, and fracture was evident. In some cases, portions of the cracked film had detached from the substrate. This solvent-induced stress cracking was not seen with 6.4×10^4 g/mol samples, however. Thus, although cracking occurred only with low MW polymer, it is not a function of MW only. As was discussed in the previous section, it may be difficult for the lower MW films to accommodate the solvent-induced stress. If the polymer structure is particularly weak, cracking will result. Perhaps cracking can be linked to residual stresses in the samples which result from poor film formation at lower MW.

The monodisperse polymer that cracked the MeOH showed no cracking in IpOH. Since the IpOH runs were performed at higher temperatures, the lack

of cracking could have been due to solvent size or temperature (or both). The larger IpOH molecules penetrate more slowly than MeOH, and so osmotic pressure does not build up as rapidly, which gives the polymer more time to relax. Furthermore, the higher temperature enhances the mobility of the polymer segments, allowing more rapid relaxation. Swelling in IpOH was not studied at lower temperatures due to prohibitively slow penetration rates.

Equilibrium Composition

The thermodynamic quality of the solvent determines the extent of swelling, i.e., ϕ_1 at equilibrium, ϕ_1^*. From Flory–Huggins theory, the difference in chemical potential between solvent in the polymer and the bulk solvent is[22]

$$\mu_1 - \mu_1^0 = RT\left[\ln(1 - \phi_2) + (1 - 1/X)\phi_2 + \chi\phi_2^2\right] \tag{7}$$

where ϕ_2 is volume fraction of polymer $(1 - \phi_1)$. At equilibrium, μ_1 in the polymer and solvent phases must be equal. If we assume that dissolution is negligible, then in the solvent phase (and thus polymer phase), $\mu_1 = \mu_1^0$, and the left side of eq. (7) goes to zero. Thus, the degree of swelling is determined by the Flory–Huggins interaction parameter. Conversely, measured values of ϕ_1^* can be used to calculate χ.

Equilibrium volume fractions were determined by fitting the ellipsometric data with the optical and transport models. Ideal mixing and 1-dimensional swelling were assumed in all cases. Composition vs. temperature is shown in Figure 10(a) for several alcohols. Values of χ were calculated using eq. (7) and the data in Figure 10(a), and these χ values are plotted vs. temperature in Figure 10(b). As expected, the equilibrium volume fraction increases with temperature [Fig. 10(a)], and equivalently χ decreases with temperature. Values of χ can be estimated from the solubility parameters of the solvent

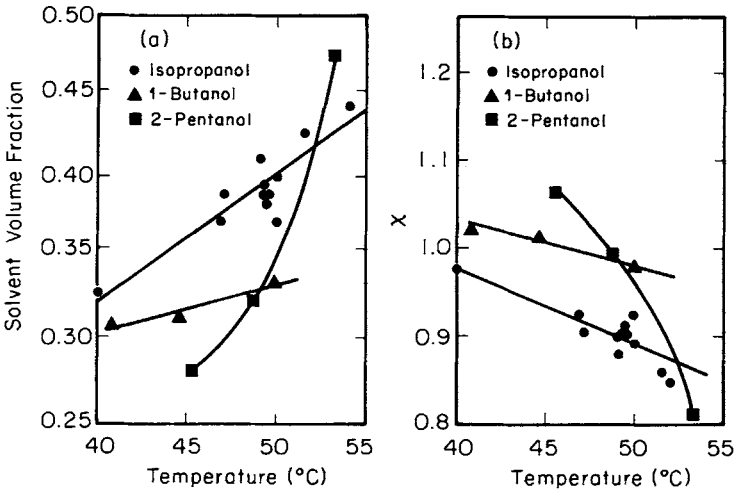

Fig. 10. Equilibrium swelling in terms of (a) ϕ_1^* and (b) χ for isopropanol, 1-butanol, and 2-pentanol.

and polymer using,[38]

$$\chi = \chi_s + \chi_h \approx 0.34 + \frac{V_1(\delta_p - \delta_s)^2}{RT} \tag{8}$$

where χ_s is the entropic contribution (assumed to be constant at 0.34), χ_h is the enthalpic contribution, and δ_p and δ_s are the solubility parameters of the polymer and solvent, respectively. Unfortunately, values of δ_p and δ_s are inexact,[38] and quantitative prediction of χ values is difficult. However, if reasonable values of the solubility parameters for PMMA and 2-pentanol are used in eq. (8), the predicted values of χ are much less sensitive to temperature than indicated by the data in Figure 10(b). The reason for this inconsistency is not clear, but perhaps the equilibrium swelling compositions converged to by the search routines correspond to local minima. More extensive studies of equilibrium swelling are required.

Transport Model Parameters

Fickian

Effective diffusivities were determined by fitting the Fickian transport model to MeOH swelling data [eq. (2)]. Both concentration-independent diffusivities and diffusivities which increase exponentially with solvent concentration were used to fit the data. For example, a concentration independent diffusivity of 10^{-11} cm^2/s was obtained at 22.3°C, which is reasonable for diffusion of MeOH in PMMA.[39] An apparent activation energy of 43 kcal/mol was determined from the concentration-independent data. This relatively high value is consistent with non-Fickian penetration, which suggests once again that MeOH diffusion involves a relaxation controlled penetrating front (high activation energy) with a significant Fickian precursor (optical data).

Case II

Values of the amplification factor a in the Case II model were determined for each solvent from average penetration velocities and eq. (3). To determine the value of a, it was necessary to first evaluate values of σ_c, K, and π. A value for the constant γ that gives the critical stress [eq. (4)] was estimated from tensile crazing data for PMMA.[40]

K as a function of temperature was determined from Case II swelling data given in Ref. 3 for PMMA in MeOH. The data consist of penetration velocity as a function of front concentration for several temperatures (23–62°C). The osmotic pressure for these data was calculated from eq. (4), and the penetration rate was plotted vs. π. Linear regression [eq. (3)] yielded values of K (and a) at each temperature. As a confirmation of the mechanical analogy, a value of K at 23°C was derived from crack-tip propagation (crazing) studies[36] ($a\pi$ is replaced with σ). This yielded a value of 3.3×10^{-10} cm/(s atm), which is in very good agreement with 2.4×10^{-10} cm/(s atm) obtained from the MeOH data.

An Arrhenius plot of K showed a break around 40°C. The apparent activation energy was 10 kcal/mol below 40°C, and 43 kcal/mol above 40°C. The parameter K is similar to a compliance, and thus creep characteristics can be used to interpret the break observed near 40°C. PMMA undergoes a secondary (β) transition from a semiductile to a ductile glass near 40°C.[41] Activation energies obtained from creep experiments are approximately 20–30 kcal/mol below T_β,[42,43] and approximately 80 kcal/mol above T_β.[43] (The activation energy below T_β corresponds to relaxation processes for side groups, whereas above T_β the activation energy corresponds to relaxation processes for polymer chains or large segments.) Although the activation energies derived from the MeOH data are much lower than those from creep experiments, in both cases the activation energies increase sharply above 40°C. Note that the activation energy for K is higher at higher temperatures, but the apparent activation energies for swelling (Fig. 6) decrease with temperature. Consequently, the parameter a must compensate for the shift in activation energy for K in order to match penetration rates.

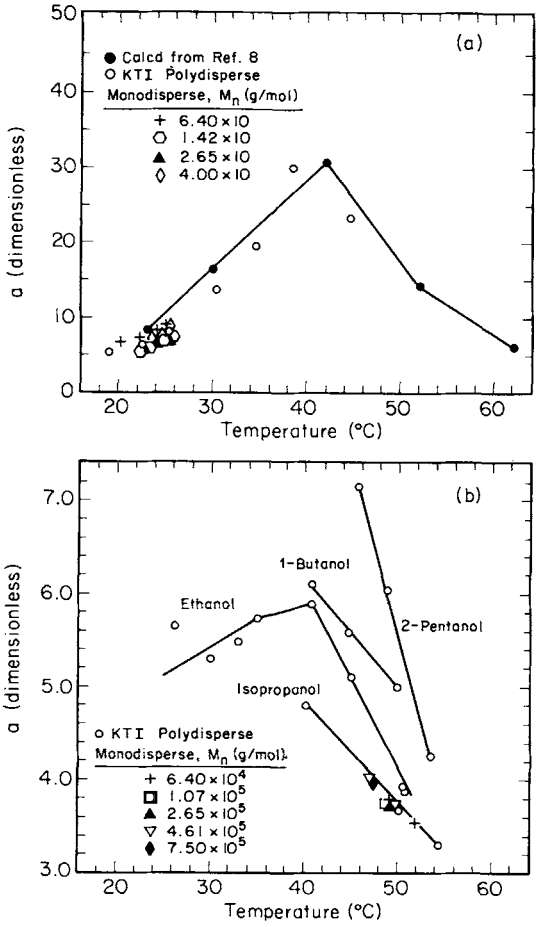

Fig. 11. Case II model parameter a vs. temperature for (a) methanol and (b) ethanol, isopropanol, 1-butanol, and 2-pentanol.

The final variable needed to calculate a was π at the front. Unlike K and σ_c, which were based on literature values, π was obtained from ellipsometric data. For the film thicknesses used in our studies, the front velocities were relatively constant, indicating that the diffusional resistance of the swollen region was negligible and that, throughout the experiment, ϕ_1 at the front was approximately ϕ_1^*. Thus, π was calculated from eq. (5) by using values of ϕ_1^* and χ that were extracted from the ellipsometric data (Fig. 10).

Values of a calculated from our data and from the data in Ref. 3 are plotted vs. temperature in Figure 11(a). (The solid line connects the points corresponding to Ref. 3. The similarity of our a values to those for Ref. 3 indicates that the penetration rates were comparable in both cases.) The values of a range from about 5 to 30, and a maximum is seen near 40°C. Other investigators[5] found that for polystyrene swelling in n-hexanes, a increased monotonically with decreasing temperature. However, for the analysis of these polystyrene data, a single activation energy was assumed (no secondary transitions), and the value of a increased with decreasing temperature merely to offset the increase in σ_c. As seen in Figure 11(a), the amplification factor is relatively insensitive to polymer molecular weight. The small variation directly reflects the dependence of penetration rate on polymer MW seen in Figure 8 (and the fact that σ_c is based onpolydisperse PMMA[40]).

Values of a for alcohols larger than MeOH are plotted in Figure 11(b). It is readily apparent that values of a for MeOH are much larger than values of a for the larger alcohols. The large deviation for MeOH is most likely due to its small molecular size, which allows it to penetrate with less relaxation by the polymer segments. This deviation is also consistent with the high degree of Fickian character seen with MeOH. Overall a cannot be assumed to be a function of only temperature. Furthermore, a consistent progression with respect to the molecular weight of the solvent is not evident, and the predictive capability of the model therefore appears limited. It must be stressed, however, that the calculated values of a are strongly dependent on the equilibrium volume fraction of solvent, and the equilibrium volume fraction does not show a consistent progression with solvent MW [Fig. 10(a)].

CONCLUSIONS

The mechanisms and kinetics of the swelling of PMMA in various alcohols have been investigated. *In situ* ellipsometry suggests that the penetration of MeOH in thin PMMA films has a high degree of Fickian character. The apparent activation energy for MeOH penetration, however, was more consistent with Case II penetration, suggesting that relaxation processes are important. Apparently, an appreciable Fickian precursor accompanies the penetrating front. EtOH penetration was primarily Case II with some Fickian character, and IpOH penetration was Case II with only a slight amount of Fickian character. Thus, Fickian character decreases with increasing solvent size.

The penetration rate of MeOH in monodisperse PMMA decreased with increasing polymer MW up to $1-2 \times 10^5$ g/mol, where the rate leveled off. The penetration rates in 6.4×10^4 g/mol monodisperse polymer were approximately twice those in 1.42×10^5 and 2.65×10^5 g/mol monodisperse sam-

ples. Further increases in MW (4.0×10^5 g/mol), however, led to increased penetration rates. The decrease in penetration rate with MW at lower MW suggests an intrinsic dependence of penetration rate on MW. The increase in penetration rate at higher MW is most likely due to increased free volume which results from the inability of the higher molecular weight chains to contract rapidly during the ambient quench. Penetration rates of MeOH in polydisperse PMMA ($M_n = 1.8 \times 10^5$ g/mol) were between those for 6.4×10^4 and 1.42×10^5 g/mol polymer. Molecular weight effects were not seen with IpOH, due to the higher temperatures at which these experiments were performed.

Some of the lower MW films cracked in MeOH (at relatively low temperatures), but for the same molecular weight samples, no cracking was observed with IpOH (elevated temperatures). The IpOH molecules cannot penetrate as readily as the smaller MeOH molecules, and furthermore at higher temperatures the polymer chains can relax more readily. Both of these factors inhibit the buildup of a catastrophic stress level. Film cracking was suppressed at higher MW, which is consistent with fracture behavior of PMMA. Not all of the lower MW films cracked, which implies that residual stresses also contribute to film cracking.

Transport parameters for Fickian and Case II swelling models were also determined. The effective concentration independent diffusivity (Fickian model) for MeOH swelling had an apparent activation energy of 43 kcal/mol, which is indicative of relaxation controlled penetration. The amplification factor a that describes the front velocity in the Case II model was found to depend on the particular solvent and on temperature. Values of this parameter were significantly higher for MeOH compared to the higher MW alcohols. This variation is probably due to the small molecular size of MeOH, and is consistent with the high degree of Fickian character seen with MeOH penetration. The dependence of a on solvent did not follow a systematic progression with the molecular weight or molar volume of the solvent. Consequently, values of a cannot be predicted from existing data by scaling with solvent size. It should be noted, however, that values of a were calculated using values of ϕ_1^*, which also failed to follow a systematic progression. If more consistent values of ϕ_1^* had been obtained, scaling of a with solvent size may have been possible.

This project was supported by the Air Force Office of Scientific Research under Grant AFOSR-90-0078. IBM 3081 and 3090 computer time was provided by an IBM DACE grant.

References

1. J. S. Vrentas and J. L. Duda, *AIChE J.*, **25**, 1 (1979).
2. T. Alfrey, Jr., E. F. Gurnee, and W. G. Lloyd, *J. Polym. Sci. C*, **12**, 249 (1966).
3. N. Thomas and A. H. Windle, *Polymer*, **19**, 255 (1978).
4. L. Nicolais, E. Drioli, H. B. Hopfenberg, and G. Caricati, *J. Membr. Sci.*, **3**, 231 (1978).
5. G. C. Sarti, *Polymer*, **20**, 827 (1979).
6. J. Manjkow, J. S. Papanu, D. W. Hess, D. S. Soane (Soong), and A. T. Bell, *J. Electrochem. Soc.*, **134**, 2003 (1987).
7. J. S. Greeneich, *J. Electrochem. Soc.*, **122**, 970 (1975).
8. A. C. Ouano, *Polym. Eng. Sci.*, **18**, 306 (1978).
9. W. J. Cooper, P. D. Krasicky, and F. Rodriquez, *Polymer*, **26**, 1069 (1985).

10. J. Manjkow, J. S. Papanu, D. S. Soong, D. W. Hess, and A. T. Bell, *J. Appl. Phys.*, **62** 682 (1987).
11. E. H. Andrews, G. M. Levy, and J. Willis, *J. Mater. Sci.*, **8**, 1000 (1973).
12. H. B. Hopfenberg, L. Nicolais, and E. Drioli, *Polymer*, **17**, 195 (1976).
13. B. R. Baird, H. B. Hopfenberg, and V. T. Stannet, *Polym. Eng. Sci.*, **11**, 274 (1971).
14. J. C. Bray and H. B. Hopfenberg, *J. Polym. Sci. B.*, **7** 679 (1969).
15. J. S. Papanu, D. S. Soane (Soong), A. T. Bell, and D. W. Hess, *J. Appl. Polym. Sci.*, to appear.
16. R. H. Muller, in *Advances in Electrochemistry and Electrochemical Engineering*, Wiley, New York, 1973, Vol. 9, pp. 167–226.
17. P. S. Hauge and F. H. Dill, *IBM J. Res. Dev.*, **17**, 472 (1973).
18. J. S. Papanu, D. S. Soane (Soong), D. W. Hess, and A. T. Bell, *J. Electrochem. Soc.*, to appear.
19. J. S. Papanu, Ph.D. dissertation, University of California, Berkeley, CA 94720, 1988.
20. F. L. McCrackin, NBS Tech. Note 479, Washington, D.C., 1969.
21. D. E. Aspnes, J. B. Theeten, and F. Hottier, *Phys. Rev. B*, **20**, 3292 (1979).
22. P. J. Flory, *Principles of Polymer Chemistry*, Cornell University Press, Ithaca, NY, 1953, p. 495.
23. G. Gergely, *Ellipsometric Tables of the Si-SiO_2 System for Mercury and He-Ne Laser Spectral Lines*, Akademia Kiado, Budapest, 1971.
24. D. F. Edwards, in *Handbook of Optical Constants of Solids*, E. D. Palik, Ed., Academic, Orlando, FL, 1985, p. 547.
25. J. Brandup and E. H. Immergut, Eds., *Polymer Handbook*, Wiley, New York, 1975, p. IV-56.
26. P. Michel, J. Dugas, J. M. Cariou, and L. Martin, *J. Macromol. Sci. Phys.*, **B25**, 379 (1986).
27. J. D. Swalen, R. Santo, M. Tacke, and J. Fischer, *IBM J. Res. Dev.*, **21**, 168 (1977).
28. R. Scheps, *J. Electrochem. Soc.*, **129**, 2273 (1982).
29. R. Scheps, *J. Electrochem. Soc.*, **131**, 540 (1984).
30. J. Timmermans, *Physicochemical Constants of Pure Organic Compounds*, Elsevier, Amsterdam, Vol. I, 1950, and Vol. II, 1965.
31. *CRC Handbook of Chemistry and Physics*, R. C. Weast, Ed., Chemical Rubber, Boca Raton, FL, 1979.
32. Y. Kohanzadeh, K. W. Ma, and J. R. Whinnery, *Appl. Opt.*, **12**, 1584 (1973).
33. H. B. Hopfenberg, *J. Membr. Sci.*, **3**, 215 (1978).
34. A. Peterlin, *J. Polym. Sci. (B)*, **3**, 1083 (1965).
35. K. Ueberreiter, in *Diffusion in Polymers*, J. Crank and G. S. Park, Eds., Academic, New York, 1968, p. 220.
36. W. Doll, in *Crazing in Polymers*, H. H. Kausch, Ed., *Adv. Polym. Sci.*, **52/53**, Springer-Verlag, Berlin–Heidelberg–New York, 1983, p. 128.
37. R. P. Kusy and M. J. Katz, *Polymer*, **19**, 1345 (1978).
38. C. J. Sheehnan and A. L. Bisio, *Rubber Chem. Technol.*, **39**, 149 (1966).
39. N. L. Thomas and A. H. Windle, *Polymer*, **23**, 529 (1982).
40. S. S. Sternstein, L. Ongchin, and A. Silverman, *Appl. Polym. Symp.*, **7**, 175 (1968).
41. S. Rabinowitz and P. Beardmore, *CRC Crit. Rev. Macromol. Sci.*, **1**, 1 (1972).
42. E. L. Morris and N. G. McCrum, *J. Polym. Sci. (B)*, **1**, 393 (1963).
43. J. A. Roetling, *Polymer*, **3**, 311 (1965).

Received January 30, 1989
Accepted February 7, 1989